Journal of Elasticity (2023) 154:407–419
https://doi.org/10.1007/s10659-023-10015-y

RESEARCH

Mechanical Response of Metal Solenoids Subjected to Electric Currents

R.S. Elliott[1] · **N. Triantafyllidis**[2,3,4]

Received: 22 January 2023 / Accepted: 8 April 2023 / Published online: 25 April 2023

Abstract
Solenoids, ubiquitous in electrical engineering applications, are devices formed from a coil of wire that use electric current to produce a magnetic field. In contrast to typical electrical engineering applications that pertain to their magnetic field, of interest here is their use as actuators by studying their mechanical deformation. An analytically tractable model of parallel, coaxial circular rings is used to find the solenoid's axial deformation when subjected to a combined electrical (current) and mechanical (axial force) loading. Both finite and infinite solenoids are considered and their equilibrium configurations as well as their stability are investigated as functions of their geometry and applied current intensity.

Keywords Deformable electric solenoid · Actuator · Stability

Mathematics Subject Classification 70H03 · 70H14 · 74F15 · 74K10 · 74M05

1 Introduction

A solenoid is a device that converts electrical to mechanical energy, using an electromagnet formed from a coil of wire. Typically, it consists of a multiturn coil of a low resistivity conducting (metallic) wire surrounded by a frame, which is also a magnetic flux carrier to enhance its efficiency. The device produces a magnetic field from electric current and in electrical engineering applications uses the magnetic field to create linear motion through a moving part, termed "*plunger*" (magnet or another coil). In mechanics applications, solenoids are used to study ductility of metals by the expansion of a thin ring-shaped specimen (see [2, 10, 11]) or in Electromagnetic Forming (EMF) (see [8, 12]). To avoid electric shorts between turns of the coil, as well as mechanical deformation, the solenoid – particularly in

✉ N. Triantafyllidis
nicolas.triantafyllidis@polytechnique.edu

1 Aerospace Engineering & Mechanics, University of Minnesota, Minneapolis, MN 55455, USA

2 LMS, École Polytechnique, CNRS UMR7649, Institut Polytechnique de Paris, Palaiseau 91128, France

3 Département de Mécanique, École Polytechnique, Palaiseau 91128, France

4 Aerospace Engineering Dept. & Mechanical Engineering Dept. (emeritus), The University of Michigan, Ann Arbor, MI 48105, USA

the case of the large currents in EMF applications – is encased in a rigid isolating and magnetically inert material, usually epoxy (e.g., see [9, 11]). Henceforth in this work the terms "*solenoid*" and "*coil*" are used interchangeably.

In contrast to the electrical engineering applications that ignore (and are conceived to prevent) mechanical deformations, of interest here is the use of electric current induced mechanical deformations for designing actuators. To the best of the authors' knowledge, no study of the mechanical deformation of a coil induced by electric current is readily accessible, in contrast to an abundance of long-established, classical work on the magnetic fields in rigid solenoids (e.g., see [3, 4]) as well as on the deformation of helicoidal springs subjected to purely mechanical loads (e.g., see [6]). To fulfill our goal of finding the mechanical response of a coil subjected to an electric current, we hereby propose an analytically tractable model of parallel, coaxial rings to investigate the solenoid's axial deformation when subjected to a combined electrical (current) and mechanical (axial force) loading.

The problem's general formulation is presented in Sect. 2. More specifically, both finite and infinite solenoids are considered, based on the well known (e.g., see [5]) analytical result of the mutual magnetic inductance of two coaxial rings subjected to an electric current. The finite extent solenoids are investigated in Sect. 2.1 while the infinite ones in Sect. 2.2. The equilibrium configurations of these coils and their stability are also investigated. It is worth mentioning that in the infinite solenoid case it will be shown that the most critical unstable mode (i.e., the one corresponding to the minimum eigenvalue of the stability operator) is a long wavelength one. We consider both naked coils as well as coils encased in a hyperelastic tube. The tube can protect against electric shorts but must be soft enough as to not adversely influence the coil's mechanical straining.

Results are presented in Sect. 3 using dimensionless quantities. In particular the influence of geometry and encasing tube's stiffness on the force–strain curves of an infinite coil are studied in Sect. 3.1. It is found that the spacing between turns as well as the encasing tube stiffness play a major role in the coil's mechanical response. Moreover, the coil's stability – determined by the sign of the force–strain curve's slope in view of the long wavelength critical mode – can change depending on the magnitude of the applied current. Analogous results for the finite solenoid case are presented in Sect. 3.2, where we study the strain distribution as a function of reference position and in particular the inevitable boundary layer.

Results for the infinite solenoid are given in dimensionless form while for finite solids some realistic values of electrical currents and geometry are used in the calculations. Moreover, the issues of what is a realistic range of stiffness ratios for the hyperelastic tubes and what is a maximum allowable electric current for different coil geometries and conducting materials are addressed respectively in Appendix A and Appendix B.

2 Problem Formulation

In this section we formulate the electromechanical deformation problem for a solenoid subjected to an electric current I and a mechanical force f_{ext} along its axis. A finite as well as an infinite case are considered and we seek the corresponding equilibrium solutions and their stability.

2.1 Finite Solenoids

A schematic representation of the coil of length L is given in Fig. 1, which consists of n turns spaced at a distance $\ell = L/n$ between them. To improve electrical insulation, the coil

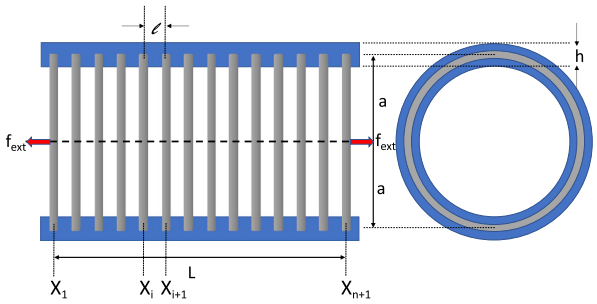

Fig. 1 Schematic of the solenoid's reference configuration; the turn i with initial position X_i in the reference configuration ($I = 0,\ f_{ext} = 0$) moves to position x_i in the current configuration ($I \neq 0,\ f_{ext} \neq 0$)

can be encased in a hyperelastic tube of thickness h. To avoid the complicated numerical calculations required for an helicoidal geometry, the solenoid is assumed to consist of identical, parallel thin rings[1] each of radius a and circular cross-section.

Assuming that the rings remain parallel and coaxial, to find the equilibrium configuration of the coil subjected to a current I and an external mechanical force f_{ext} one has to determine the current positions x_i of the rings, initially at X_i as indicated in Fig. 1. To this end we minimize the system's potential energy $\mathcal{P}$, which consists of a mechanical part $\mathcal{W}_{\text{mec}}$, an electrical part $\mathcal{W}_{\text{elec}}$ and an external contribution $\mathcal{W}_{\text{ext}}$ due to the applied (and opposite) mechanical forces $\pm f_{\text{ext}}$ at the two ends of the solenoid along its axial direction.

$$\mathcal{P} \equiv \mathcal{W}_{\text{mec}} + \mathcal{W}_{\text{elec}} + \mathcal{W}_{\text{ext}}\,. \tag{2.1}$$

The mechanical energy consists of the energy stored in the coil[2] plus the energy of the hyperelastic encasing tube (assumed neo-Hookean).

$$\mathcal{W}_{\text{mec}} = \sum_{1\le i\le n} \left\{ \frac{k_s}{2}(x_{i+1} - x_i - \ell)^2 + \frac{A_t G_t \ell}{2}[(\lambda_i)^2 + 2(\lambda_i)^{-1} - 3] \right\}, \quad \lambda_i \equiv (x_{i+1} - x_i)/\ell\,. \tag{2.2}$$

In the above expression the first (quadratic) term represents the elastic energy of the (naked) coil associated with the change of spacing between two adjacent turns and k_s denotes the corresponding stiffness. The second term is the elastic energy associated with the change of length of a section of the encasing tube[3] of initial (at zero stress) shear modulus G_t, initial length ℓ and cross sectional area $A_t = 2\pi a h,\ (h \ll a)$ while λ_i is the corresponding stretch ratio for that section of the tube.

The electric energy is due to the interaction of all rings and given by (see [5])

$$\mathcal{W}_{\text{elec}} = -\sum_{1\le i,j\le n+1} \left\{ \frac{I^2}{2}\mu_0\, L_{ij} \right\}; \quad L_{ij} = \begin{cases} 2a\mathcal{F}(z_{ij}), & \text{for } i \neq j, \\ c_i, & \text{for } i = j, \end{cases} \tag{2.3}$$

where $\mathcal{F}(z) \equiv [(1 - z^2/2)K(z) - E(z)]/z$, and $z_{ij} \equiv [1 + ((x_i - x_j)/2a)^2]^{-1/2}$ for $i \neq j$. The functions $K(z)$ and $E(z)$ entering the expression for the *mutual inductance* L_{ij} are,

[1] It should be noted here that a coil with parallel rings can also be realized experimentally (see [7]).

[2] Due to the small pitch angle of the solenoid coils considered here, even for relatively large relative displacements e_i between turns ($e_i \equiv \lambda_i - 1$) — in Sect. 2.2 we consider up to $|e_i| = |e| = 0.5$ — the force-displacement relation for the coil is assumed to remain linear. Large strain nonlinear effects are taken into account in the hyperelastic encasing tube which provides a stiffening response with increasing e.

[3] The tube is assumed incompressible neo-Hookean and in a uniaxial stress state; different constitutive laws could easily be considered.

respectively, the *complete elliptic integrals of the first and second kind*. Notice that only the mutual inductance terms $i \neq j$ need to be considered in the electric energy, as the energy stored due to the self-inductance $L_{ii} = c_i$ is independent of the coil deformation.[4]

It is useful for the subsequent derivations to give the definitions for the complete elliptic integrals of the first and second kind and their derivatives (e.g. see [1]).

$$\begin{aligned} K(z) &\equiv \int_0^{\pi/2} [1 - z^2 \sin^2 x]^{-1/2} dx \,, \qquad E(z) \equiv \int_0^{\pi/2} [1 - z^2 \sin^2 x]^{1/2} dx \,, \\ \frac{dK(z)}{dz} &= [E(z)/(1 - z^2) - K(z)]/z \,, \qquad \frac{dE(z)}{dz} = [E(z) - K(z)]/z \,. \end{aligned} \tag{2.4}$$

Finally the external contribution $\mathcal{W}_{\text{ext}}$ from the mechanical forces $\pm f_{\text{ext}}$ at the ends of the solenoid is

$$\mathcal{W}_{\text{ext}} = -(x_{n+1} - x_1 - L) f_{\text{ext}} \,. \tag{2.5}$$

For given values of I and f_{ext}, the system's equilibrium equations are obtained by extremizing $\mathcal{P}(x_i; I, f_{\text{ext}})$

$$\frac{\partial \mathcal{P}}{\partial x_i} = 0 \,, \quad 1 \leq i \leq n+1 \,. \tag{2.6}$$

Note that if $x_i(I, f_{\text{ext}})$ is a solution to (2.6), then $x_i(I, f_{\text{ext}}) + c$, $\forall c \in \mathbb{R}$ is also a solution to the same equilibrium equations since a rigid body translation of the system leaves its energy invariant, as verified by inspection of the expressions for the energies in (2.2), (2.3), and (2.5). This translation invariance of (2.6) is eliminated by adding a penalty term to the potential energy, i.e., taking $\mathcal{P} + (1/2)(\sum x_i)^2$.

Solutions to the above equations are obtained numerically by an incremental Newton–Raphson method for the applied current I and force f_{ext}. The initial guess for x_i is obtained by using the fact that in the absence of electric current ($I = 0$), all turns of the solenoid are equally spaced[5] $x_{i+1} - x_i = \ell(1 + e)$ and $e = k_s f_{\text{ext}}/\ell$, where e is the corresponding uniform strain.

The stability of the thus obtained equilibrium solution is established by investigating the positive definiteness of the second derivative of the penalized potential energy $\partial^2 \mathcal{P}/\partial x_i \partial x_j$ evaluated on the equilibrium solution of interest, i.e., whether the minimum eigenvalue of this matrix is positive. This stability criterion assumes the dynamics of electric currents are not important and, thus, that $\mathcal{P}$ serves as a potential energy for which the Principle of Minimum Potential Energy is applicable.

2.2 Infinite Solenoids

Analytical results can be obtained by considering an infinite solenoid. In addition to the interest of this problem for its own merit, it provides an independent verification of the numerical calculations for the finite solenoids when the number of turns $n \to \infty$ by comparing the infinite solenoid results to those of the middle section (i.e., away from the boundaries) of a finite solenoid with the same coil geometry and subjected to the same electric current.

[4] The self-inductance of a circular ring of radius a is a constant $L_{ii} = c_i$ that depends only on the coil wire's cross-sectional geometry; $c_i = a[\ln(8a/\rho) - 7/4]$ for a circular section of radius ρ (e.g., see [5, 10]).

[5] For simplicity the naked coil ring spacing is given but the uniform strain solution e in the presence of an encasing hyperelastic tube is a straightforward solution of (2.6).

In the fundamental solution of the infinite solenoid all coils displace by the same relative amount ℓe, where e is the coil's uniform strain, and thus the deformed spacing between two rings is

$$x_{i+q} - x_i = q\ell(1+e)\,; \quad q \in \mathbb{Z}\,. \tag{2.7}$$

For the infinite solenoid we need the potential energy per unit cell, calculated by appropriately adapting, with the help of (2.7), the expressions for the mechanical and electric energies in (2.2) and (2.3), respectively. One obtains the following expression for the potential energy per unit cell (also denoted by $\mathcal{P}$ for simplicity), i.e., one ring and the surrounding elastic tube segment of initial (reference configuration) length ℓ

$$\mathcal{P} = \frac{k_s}{2\ell}(\ell e)^2 + \frac{A_t G_t}{2}[(1+e)^2 + 2(1+e)^{-1} - 3] - I^2\mu_0(\frac{2a}{\ell})\sum_{q=1}^{q=Q}\mathcal{F}(z_q(e)) - f_{\text{ext}}e\,,$$

$$z_q(e) \equiv [1 + (q\ell(1+e)/2a)^2]^{-1/2}\,, \tag{2.8}$$

with $Q \in \mathbb{N}$ the maximum number of rings influencing the stored electric energy in either direction of the cell and hereinafter referred to as the "*range number*".

Switching from the force-control formulation of (2.8) to a strain (e control) formulation, the internal force–strain relation of the infinite solenoid[6] is given by:

$$\begin{aligned} f \equiv \frac{d\mathcal{P}}{de} &= k_s\ell e + A_t G_t[(1+e) - (1+e)^{-2}] \\ &\quad - I^2\mu_0(\frac{\ell}{2a})\sum_{q=1}^{q=Q} z_q(e)\left[K(z_q(e)) - E(z_q(e))\frac{1 - z_q^2(e)/2}{1 - z_q^2(e)}\right]q^2\,. \end{aligned} \tag{2.9}$$

The stability of the fundamental solution is found by examining the sign of the minimum eigenvalue $\beta_{min}(e)$ of the second derivative of the potential energy for a given e. Using the Bloch–Floquet theory for representing all possible bounded perturbations of the translationally-invariant infinite system, the corresponding eigenvalue $\beta(\omega; e)$ is found to satisfy

$$\begin{aligned} &\beta(\omega; e)\delta x_i = \sum_{q=-Q}^{q=+Q}\left.\frac{\partial^2\mathcal{P}}{\partial x_i \partial x_{i+q}}\right|_e \delta x_{i+q}\,, \quad \delta x_{i+q} = \delta x_i \exp[2\pi\,\mathrm{i}\omega q]\,, \\ &\omega \in (0,1]\,, \quad q \in \mathbb{Z}\,, \quad Q \in \mathbb{N}\,, \end{aligned} \tag{2.10}$$

where $\mathrm{i} = \sqrt{-1}$ denotes the imaginary unit, ωq represents the perturbation's frequency, and $\mathcal{P}$ refers to the potential energy of an infinite solenoid. Note that the long (much larger than the unit cell) wavelength $(1/\omega q)$ perturbations correspond to $\omega \longrightarrow 0$. Taking advantage of the existence of a potential energy and its translational invariance in the x-direction (i.e., $\partial^2\mathcal{P}/\partial x_i \partial x_{i+q} = \partial^2\mathcal{P}/\partial x_i \partial x_{i-q}$), using the properties of the elliptic integrals in (2.4), one

[6] An externally applied reaction force $f_{ext} = f$ is needed for maintaining the applied strain e.

obtains from (2.8) and (2.10) the following expression for the eigenvalue $\beta(\omega; e)$

$$\begin{aligned}
&\beta(\omega; e) = [1 - \cos(2\pi\omega)] \left\{ M(e) - \sum_{q=1}^{q=Q} C_q(e) \left[\frac{1 - \cos(2\pi\omega q)}{1 - \cos(2\pi\omega)} \right] \right\} , \\
&M(e) \equiv k_s + \frac{A_t G_t}{\ell} [1 + 2(1+e)^{-3}] , \\
&C_q(e) \equiv I^2 \mu_0 \frac{z_q^3(e)}{2a} \left[\frac{K(z_q(e))}{2} + E(z_q(e)) \frac{z_q^2(e) - 1/2}{1 - z_q^2(e)} \right] ,
\end{aligned} \tag{2.11}$$

where $z_q(e)$ is defined in (2.8).

One can verify that $M(e) > 0$ and $C_q(e) > 0$, $\forall q \in \mathbb{N}$. The ratio $(1 - \cos(2\pi\omega q))/(1 - \cos(2\pi\omega)) > 0$ is positive for all ω and is maximized as $\omega \longrightarrow 0$, where its leading asymptotic term becomes q^2. Thus, the minimum eigenvalue always occurs near $\omega = 0$, and in this neighborhood we have[7]

$$\beta(\omega; e) = 2(\pi\omega)^2 B(e) , \quad B(e) \equiv M(e) - \sum_{q=1}^{q=Q} C_q(e) q^2 . \tag{2.12}$$

Consequently the principal solution of the infinite solenoid is stable when the curvature of the $\beta(\omega; e)$ curve is positive, i.e., when $B(e) > 0$. The first instability occurs for a long wavelength mode ($\omega \longrightarrow 0$) immediately after $B(e) = 0$ (when $B(e) < 0$). The stability criterion for the long wavelength mode can be independently obtained by taking the second e-derivative of the unit cell potential energy, defined in (2.8)

$$\frac{d^2\mathcal{P}(e)}{de^2} = \ell B(e) , \tag{2.13}$$

where $B(e)$ is defined by (2.12). An important conclusion from (2.9) is that the stability of the infinite solenoid is given by the slope of the force–strain curve since $df/de = d^2\mathcal{P}(e)/de^2 = \ell B(e)$.

3 Results and Discussion

All results in this section are presented in non-dimensional form using the following variables for geometry R, current J, tube stiffness S, and force F

$$R \equiv a/\ell , \quad J \equiv I\,(k_s \ell/\mu_0)^{-1/2} , \quad S \equiv (A_t G_t/k_s \ell) , \quad F \equiv f/(k_s \ell) . \tag{3.1}$$

3.1 Infinite Solenoid

Using the above-defined dimensionless quantities, we solve the strain-control infinite solenoid equilibrium equation in (2.9) to obtain the corresponding force–strain response for different geometries and applied currents and the results are presented in Fig. 2 and Fig. 3. More specifically in Fig. 2 we investigate the influence of geometry for $10 \leq R \leq 100$ and

[7] As expected from translational invariance, an eigenvalue $\beta = 0$ always exists and corresponds to $\omega = 0$ (see also (2.11)).

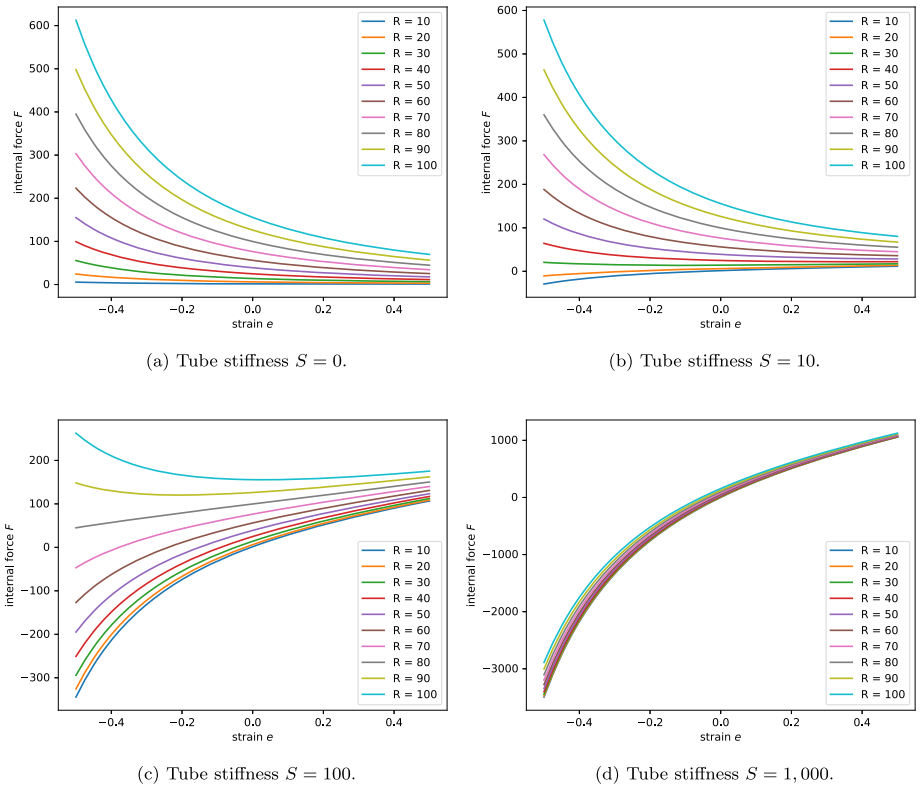

(a) Tube stiffness $S = 0$.

(b) Tube stiffness $S = 10$.

(c) Tube stiffness $S = 100$.

(d) Tube stiffness $S = 1,000$.

Fig. 2 Influence of dimensionless radius $R \equiv a/\ell$ on the force–strain curves in an infinite solenoid for different stiffnesses $S \equiv A_t G_t / k_s \ell$ of the encasing hyperelastic tube. All calculations correspond to a fixed dimensionless current $J = 0.1$. The stability of the infinite solenoid is given by the slope of these curves: positive (negative) slope corresponds to a stable (unstable) solenoid

tube stiffness $0 \leq S \leq 1,000$ on the force–strain curves under a fixed dimensionless current $J = 0.1$. In all calculations for Fig. 2 a range number $Q = 1,600$ is used to ensure a convergence accuracy for the equilibrium internal force f of 10^{-5}. Recall that the stability of the infinite solenoid is given by the slope of the force–strain curves: positive (negative) slope corresponds to a stable (unstable) solenoid, since the long wavelength (much larger than the unit cell) is always the critical mode, as shown in Sect. 2.2. Notice that for the naked ($S = 0$) solenoid in Fig. 2a the electric current influence increases significantly with increasing R, the dimensionless reference inverse-spacing between turns. Moreover, from the remark made following (2.13), the naked solenoid is always unstable, for sufficiently large electric current. A ten-fold increase in the tube stiffness ($S = 10$) presented in Fig. 2b shows no significant difference from the naked coil case in Fig. 2a for large values of $R \geq 70$ but an important impact for the lower values $R \leq 20$ that leads to stable equilibria of the corresponding solenoids.

The situation changes considerably for the case of a much stiffer encasing tube that stabilizes the infinite coil with the larger spacings – positive slopes of the force–strain curves for $10 \leq R \leq 80$ – as recorded in Fig. 2c for $S = 100$. Finally the solenoid with the stiffest encasing tube $S = 1,000$ is always stable independently of the spacing between turns, as observed in Fig. 2d.

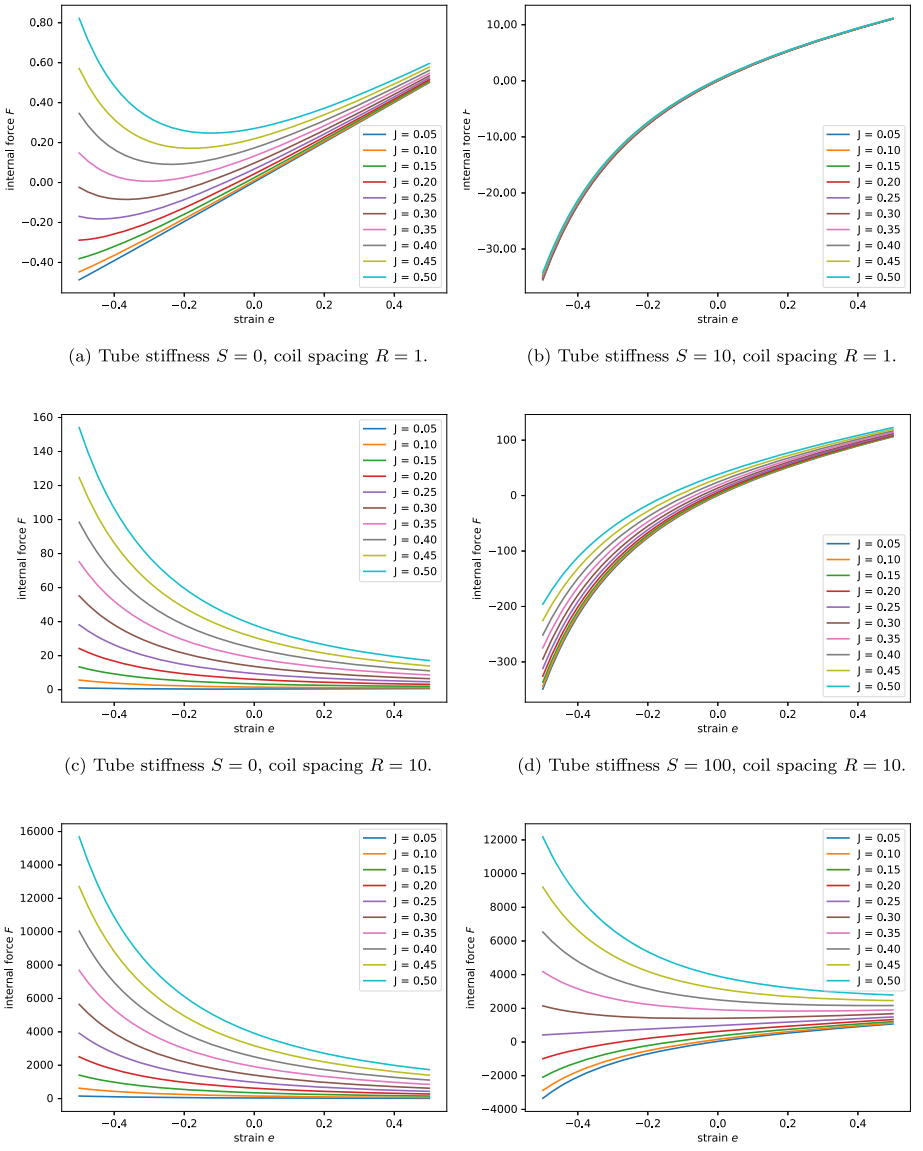

(a) Tube stiffness $S = 0$, coil spacing $R = 1$.

(b) Tube stiffness $S = 10$, coil spacing $R = 1$.

(c) Tube stiffness $S = 0$, coil spacing $R = 10$.

(d) Tube stiffness $S = 100$, coil spacing $R = 10$.

(e) Tube stiffness $S = 0$, coil spacing $R = 100$.

(f) Tube stiffness $S = 1,000$, coil spacing $R = 100$.

Fig. 3 Influence of the dimensionless current J on the force–strain curves in an infinite solenoid for different stiffnesses $S \equiv A_t G_t / k_s \ell$ of the encasing hyperelastic tube and different dimensionless radii $R \equiv a/\ell$. The stability of the infinite solenoid is given by the slope of these curves: positive (negative) slope corresponds to a stable (unstable) solenoid

In Fig. 3 we investigate the influence of the dimensionless current J on the force–strain curves for different coil geometries ($R = 1, 10, 100$) and tube stiffnesses ($S = 0, 10, 100, 1000$). In these calculations, and depending on the coil dimensionless radius R, a range number $Q = 1,600$ is necessary for the coil with the largest spacing between turns

($R = 1$), a range number $Q = 12,800$ is necessary for the coil with the intermediate spacing between turns ($R = 10$) and a much higher range number $Q = 102,400$ is needed for the coil with the closest spacing between turns ($R = 100$) to ensure a convergence accuracy for the equilibrium force f of 10^{-5}.

By comparing the coils with the largest spacing between turns ($R = 1$), one sees from Fig. 3a that in the naked case ($S = 0$) the coil is unstable for applied currents $J > 0.2$ and strains lower than $e < 0.4$. Upon increasing the current one requires higher strains to stabilize the coil. The addition of a relatively soft encasing tube ($S = 10$) has a strong stabilizing effect on the solenoid, as seen in Fig. 3b, where all force–strain curves essentially coincide with the response of the hyperelastic encasing tube and are practically unaffected by the electric currents.

For solenoids with an intermediate turn spacing ($R = 10$) one sees for the naked case in Fig. 3c that the solenoid is unstable for all applied currents, while the addition of a hyperelastic tube with $S = 100$ reverses the situation by stabilizing the coil for all currents, as seen in Fig. 3d. For the coils with the smallest spacing between turns ($R = 100$), the naked ones are always unstable according to Fig. 3e, while it takes an encasing hyperelastic tube with considerably higher stiffness ($S = 1,000$) to stabilize it for lower current values of $J \leq 0.25$, as seen in Fig. 3f.

3.2 Finite Solenoid

In order to give a practical view[8] for the deformation of a solenoid subjected to an electric current I, we present in this section results for three naked ($A_t = 0$), helicoidal solenoids, all of radius $a = 5 \times 10^{-2}$ m, made of copper ($E_s = 160 \times 10^9$ Pa, $\nu_s = 1/3$) wire of radius $\rho = 10^{-3}$ m with lengths $L = a,\ 10a,\ 40a$. No end forces are applied ($f_{\text{ext}} = 0$) resulting in contraction (strains $e < 0$). For each coil we consider two different number of turns $n = 50,\ 100$ and the spacing between two turns is $\ell = L/n$.

The stiffness k_s for a helicoidal spring of pitch angle $\alpha = \arctan(\ell/2\pi a)$ is given by (e.g., see [6])

$$\text{helicoidal solenoid stiffness:} \quad k_s = \frac{\rho^4}{(2a)^3} \frac{E_s \cos\alpha}{1 + \nu_s \cos^2\alpha}\,. \tag{3.2}$$

The influence of the applied current I on the deformed shape for the above-described finite solenoids is presented in Fig. 4 which depicts the strain distribution along each solenoid, defined as the change of spacing between two rings divided by the initial ring spacing, i.e., $(x_{i+1} - x_i - \ell)/\ell$. All cases presented here pertain to stable solutions, as the minimum eigenvalue of the stability matrix is positive (see discussion following (2.6) at the end of Sect. 2.1).

More specifically, we compare the deformed shapes of same length L solenoids subjected to the same current I but with a different number of turns n and hence with different coil densities. In Fig. 4a and Fig. 4b we compare two solenoids of $n = 50$ and $n = 100$ turns, respectively, both with the same total length $L = 40a$ and subjected to a current $I = 150$ A. In Fig. 4c and Fig. 4d we compare two solenoids of $n = 50$ and $n = 100$ turns, respectively, both with the same total length $L = 10a$ and subjected to a current $I = 20$ A. Finally, in Fig. 4e and Fig. 4f we compare two solenoids of $n = 50$ and $n = 100$ turns, respectively, both with the same total length $L = a$ and subjected to a current $I = 1$ A. To relate results

[8] Standard MKSA system of units is used in this subsection.

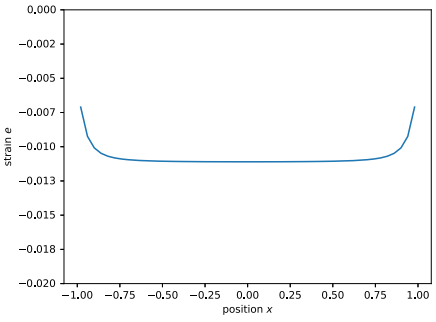

(a) Turns $n = 50$, length $L/a = 40$, current $I = 150$ A (Dimensionless: spacing $R = 1.25$, current $J = 0.0768$).

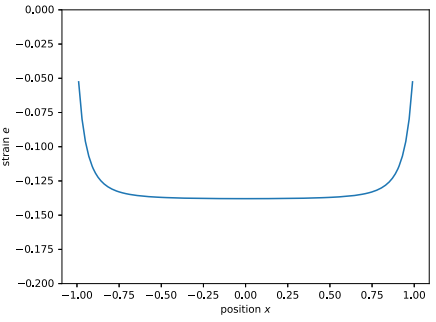

(b) Turns $n = 100$, length $L/a = 40$, current $I = 150$ A (Dimensionless: spacing $R = 2.5$, current $J = 0.1084$).

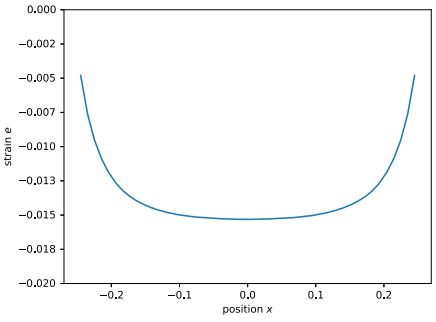

(c) Turns $n = 50$, length $L/a = 10$, current $I = 20$ A (Dimensionless: spacing $R = 5.0$, current $J = 0.02044$).

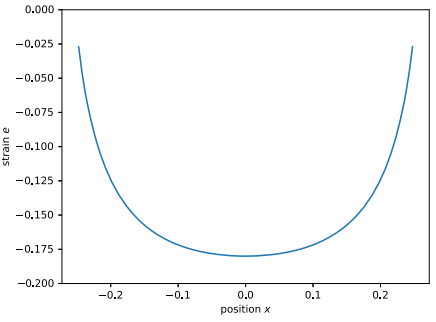

(d) Turns $n = 100$, length $L/a = 10$, current $I = 20$ A (Dimensionless: spacing $R = 10.0$, current $J = 0.02891$).

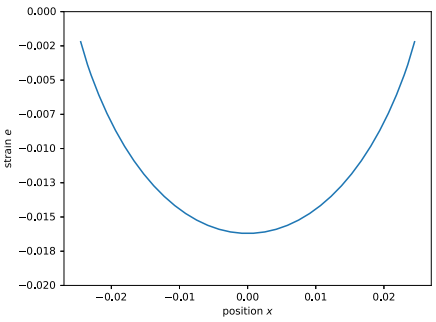

(e) Turns $n = 50$, length $L/a = 1$, current $I = 1$ A (Dimensionless: spacing $R = 50.0$, current $J = 0.003232$).

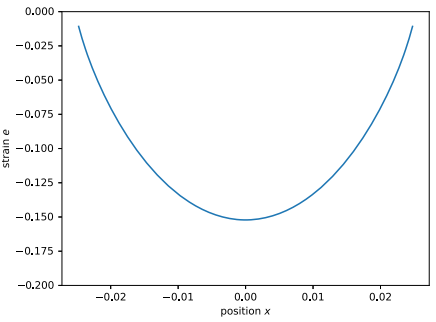

(f) Turns $n = 100$, length $L/a = 1$, current $I = 1$ A (Dimensionless: spacing $R = 100.0$, current $J = 0.004571$).

Fig. 4 Influence of number of coils n on the strain profile in naked, unconstrained (i.e., no end forces) helicoidal solenoids, all of radius $a = 5$ cm and made of copper wire of radius $\rho = 1$ mm. The subfigures in each row correspond to coils that have the same length and current. Note the different strain scales between the two columns. The figures in each column correspond to coils that have the same number of turns. All equilibrium solutions are found to be stable

to the previous subsection, the corresponding dimensionless radius R and current J are also given in parentheses at the caption below each subfigure.

It should be noted at this point that the maximum pitch angle of these helicoidal solenoids is rather small ($\alpha \approx 7^\circ$, which corresponds to the longest solenoid: $L/a = 40$ with the smaller number of turns: $n = 50$), thus justifying the parallel ring assumption made in Sect. 2.

Notice that as the spacing between turns decreases (going from top to bottom rows) the large uniform strain zone at the middle of the coil progressively disappears since a larger number of rings strongly interact due to the shorter distance between them for the denser coils. On the contrary obtaining the same maximum strain requires a lower current for the higher density solenoid, as one can observe by comparing the three different rows (from top to bottom) in Fig. 4. Additionally, as expected, for the same current the strains are considerably lower (about an order of magnitude) for the coils with the lower number of turns, as a comparison of the subfigures on the left and right rows of Fig. 4. The maximum strain in each case can be adequately approximated by the infinite solenoid calculations in Sect. 2.2 with the best approximation corresponding to the longest coil $L/a = 40$ ($e \approx 0.0115$ for $n = 50$ turns and $e \approx 0.137$ for $n = 100$ turns).

A remark is also in order at this point, pertaining to the influence of an externally applied force f_{ext}. Not surprisingly, our calculations show that the presence of external forces leads to the addition of a uniform strain e, resulting in a simple shift (up or down along the y-axis depending on the sign of the applied external force) of the curves in Fig. 4, thus justifying the absence of corresponding additional plots.

4 Conclusion

In contrast to the electrical engineering applications, we are interested here in solenoids as actuators by exploiting their mechanical deformation resulting from an electric current. Since – to the best of the authors' knowledge – the mechanical deformation of a coil induced by current have not been the object of previous investigations in the engineering literature, we present an analytically tractable model of parallel, coaxial rings to find the solenoid's axial deformation when subjected to a combined electrical (currents) and mechanical (axial forces) loading. We consider both naked coils as well as coils encased in hyperelastic tubes, as the latter case can protect against electric shorts but be soft enough to not significantly influence the coil's mechanical straining.

We study the equilibrium configurations and stability of both finite and infinite solenoids and find that in the latter case the critical unstable mode, i.e., the one minimizing the lowest eigenvalue of the stability operator for a given geometry and current, is a long wavelength one; consequently the stability of the infinite solenoid is determined by the slope of the force–strain curves: positive (negative) slope corresponds to a stable (unstable) solenoid. It should be noted that in the case of finite solenoids we account for the interaction of all rings while for the case of infinite solenoids we account for the necessary number of rings needed to find the equilibrium force with a prescribed accuracy.

It is found that the spacing between turns as well as the encasing tube stiffness play a major role in the coil's mechanical response. Moreover, the coil's stability can change depending on the magnitude of the applied current. Analogous results for the finite solenoid case are obtained by studying the strain distribution as a function of position, where we find that the size of the strain boundary layer increases as the spacing between turns decreases.

Appendix A: Naked and Tube-Encased Coil Stiffnesses

The stiffness of the naked solenoid depends on its geometry. For the helicoidal coil the stiffness k_s is given by (3.2). For the parallel ring naked solenoid, the stiffness of the separating ligament is

$$\text{parallel ring solenoid stiffness:} \quad k_s = \frac{E_s \pi \rho^2}{\ell} \,. \tag{A.1}$$

Assuming a minimum encasing tube thickness of $h = 2\rho$, we conclude from the definitions in (3.1) of the dimensionless tube stiffness parameter S and the aspect ratio R that

$$\text{helicoidal solenoid:} \quad S = 8\pi R \left(\frac{2a}{\rho}\right)^3 \frac{G_t}{G_s} \,; \quad \text{parallel rings:} \quad S = \frac{2a}{\rho}(1+\nu_s)\frac{G_t}{G_s} \,. \tag{A.2}$$

For soft polymeric tubes and metallic solenoids (typically copper) the ratio is of the order $G_t/G_s \approx 10^{-3}$ while a typical value[9] of the ratio $\rho/2a \approx 10^{-2}$, thus justifying the range of values for S used in the calculations of Sect. 3.

Appendix B: Electric Current Limitations

Finally, an interesting question can be raised on the subject of any physically imposed limits to the magnitude of the applied currents. Two physical mechanisms are here at play: the dielectric resistance of the medium in which the solenoid is encased and the ohmic heating of the solenoid wire. We bypass the first issue under the hypothesis of good electrical isolating properties of the encasing tube and address here the limitations due to the second mechanism.

Assuming a complete conversion of ohmic losses to heat in a circular section of radius ρ wire of conductivity γ, mass density m and specific heat c_p we have that the maximum current $I_{\max}$ allowed by an increase of temperature rate $\dot{\theta}_{\max}$

$$I_{\max} = \pi \rho^2 (\gamma m c_p \dot{\theta}_{\max})^{1/2} \,. \tag{B.1}$$

For a coil made of copper wire (in MKSA units: $m = 8.94 \times 10^3$, $\gamma = 5.96 \times 10^7$, $c_p = 0.385 \times 10^3$) of radius $\rho = 10^{-3}$ (the dimensions considered in Sect. 3.2) we have the following maximum current

$$I_{\max} \approx 45 (\dot{\theta}_{\max})^{1/2} \text{ A} \,. \tag{B.2}$$

Consequently assuming $\dot{\theta}_{\max} = 1^\circ/\text{sec}$ the maximum current can be $I_{\max} \approx 45$ A while for $\dot{\theta}_{\max} = (10^{-2})^\circ/\text{sec}$ the corresponding $I_{\max} \approx 4.5$ A, thus giving an estimate of how fast the three different solenoids of Sect. 3.2 are heating.

Acknowledgements This work is dedicated to a good friend and an excellent scholar, Prof. Roger Fosdick on the occasion of his 85th birthday.

Author contributions Ryan Elliott and Nicolas Triantafyllidis have both contributed in the concept of the work, calculations and writing of the manuscript.

[9] In Sect. 3.2 a coil of diameter $2a = 10^{-1}$ m is considered with a wire of thickness $\rho = 10^{-3}$ m.

Declarations

Competing interests The authors declare no competing interests.

References

1. Abramowitz, M., Stegun, I.: Handbook of Mathematical Functions. Dover, New York (1965)
2. Gourdin, W.H.: Analysis and assessment of electromagnetic ring expansion at a high-strain-rate test. J. Appl. Phys. **65**, 411–422 (1989)
3. Griffiths, D.: Introduction to Electrodynamics. Pearson Education, Upper Saddle River (2014)
4. Jackson, J.D.: Classical Electrodynamics, 3rd edn. Wiley, New York (1999)
5. Kovetz, A.: Electromagnetic Theory. Oxford University Press, London (2000)
6. Love, A.E.H.: A Theasise on the Mathematical Theory of Elasticity. Dover, New York (1944)
7. Mainy, A.: Dynamic buckling of thin metallic rings under external pressure. Master's thesis, University of Texas (2012)
8. Thomas, J., Triantafyllidis, N.: On electromagnetic forming processes in finitely strained solids: theory and examples. J. Mech. Phys. Solids **57**(8), 1391–1416 (2009)
9. Thomas, J.D., Seth, M., Bradley, J., Daehn, G., Triantafyllidis, N.: Forming limits for electromagnetically expanded aluminum alloy tubes: theory and experiment forming limits for electromagnetically expanded aluminum alloy tubes: theory and experiment. Acta Mater. **55**, 2863–2873 (2007)
10. Triantafyllidis, N., Waldenmyer, J.: Onset of necking in electro-magnetically formed rings. J. Mech. Phys. Solids **52**, 2127–2148 (2004)
11. Zhang, H., Ravi-Chandar, K.: On the dynamics of necking and fragmentation – I. Real-time and post-mortem observations in Al 6061-O. Int. J. Fract. **142**, 183–217 (2006)
12. Zhang, H., Ravi-Chandar, K.: On the dynamics of necking and fragmentation – IV. Expansion of Al 6061-O tubes. Int. J. Fract. **163**, 41–65 (2010)